Analyst

PAPER

View Article Online
View Journal

Cite this: DOI: 10.1039/c4an01171f

Dual amplification of single nucleotide polymorphism detection using graphene oxide and nanoporous gold electrode platform†

Seyyed Mehdi Khoshfetrat and Masoud A. Mehrgardi*

In the present manuscript, a strategy to prompt the sensitivity of a biosensor based on the dual amplification of signal by applying a nanoporous gold electrode (NPGE) as a support platform and soluble graphene oxide (GO) as an indicator has been developed. By increasing the surface area of the biosensing platform and because of unique GO/ss-DNA interactions, the sensitivity for the detection of SNPs is enhanced. In the presence of SNPs, because of less effective hybridization of mutant targets compared to complementary targets, further GO could adsorb on mutant targets-modified NPGE *via* $\pi-\pi$ interactions, causing a large increase in the charge transfer resistance (R_{ct}) of the electrode. This protocol provides a cost-effective and fast method for the discrimination of different SNPs. Furthermore, this biosensor can detect thermodynamically stable SNP (G–T mismatches) in the range of 15–1600 pM. The present strategy is a label-free and sensitive protocol and does not require sophisticated fabrication.

Received 30th June 2014
Accepted 22nd July 2014

DOI: 10.1039/c4an01171f

www.rsc.org/analyst

1. Introduction

Fast and simple determination of specific sequences of deoxyribonucleic acid (DNA) at low concentrations, particularly methods for the rapid identification of base mutations or single nucleotide polymorphisms (SNPs), would prove useful in the diagnosis of several genetic diseases and for clinical, forensic and pharmaceutical applications.[1] Electrochemical techniques can provide significant advantages over other existing devices because of their simplicity, rapidness, low-cost, high sensitivity and selectivity.[2] One of the key steps for the fabrication of DNA electrochemical biosensors is determining the amount and stability of the immobilized single-stranded DNA (ss-DNA) probes as well as the accessibility of target DNA toward the electrode with immobilized probe DNA.[3] Therefore, increasing the immobilization amount and controlling the molecular orientation of ss-DNA improves the performance of DNA biosensors.[4] So far, numerous immobilization strategies have been reported and employed for increasing the amount of immobilized DNA. The introduction of a nanomaterial could effectively increase the electrode surface area and enhance the amount of immobilized DNA.[5] Cai *et al.*[6] assembled AuNPs on a cysteamine-modified gold electrode and demonstrated that the immobilization quantities of thiolated probe DNA on the modified electrode are largely increased compared to a bare gold electrode. Kelley and co-workers[7] developed a strategy for the controlled fabrication of nanowire and Pd nanostructure modified electrodes and achieved more sensitive DNA detection by controlling the orientation of the DNA probe. Hu co-workers[8] developed an electrochemical DNA biosensor based on a nanoporous gold electrode and multifunctional encoded DNA–Au bio barcodes. Our research group recently reported a strategy for the detection of thermodynamic single base mismatches using a nanoporous gold electrode (NPGE).[9] Because of prominent properties, such as high specific surface area, biocompatibility, excellent conductivity, chemical and thermal stability and toxicological safety, NPGEs are attractive platforms for the immobilization of biocomponents.[10,11] Because the methods for the preparation of NPGEs, such as template-directed synthesis,[12] hydrothermal treatment,[13] and electrochemical/chemical dealloying,[14,15] usually involve complex procedures, their applications for signal amplification of DNA in electrochemical biosensors are limited.[16] A simple strategy for the construction of nanoporous modified electrodes to achieve high sensitivity is extremely desirable. Recently, some new facile electrochemical strategies have been reported for the fabrication of NPGEs.[17–20] As a nanostructure biointerface, *in situ* prepared NPGEs are appropriate for the construction of electrochemical biosensors because of the ease of manipulation and high stability. Much more attention has been focused on the sensitivity enhancement for the detection of DNA hybridization based on the avidin-hydrazine label,[21] functionalized liposome,[22] redox-active reporter molecule and enzyme label,[23] and metal/semiconductor nanoparticle label.[24,25]

While these methods generally have suitable detection limits, their practical application is restricted due to complicated

Department of Chemistry, University of Isfahan, Isfahan 81746-73441, Iran. E-mail: m.mehrgardi@chem.ui.ac.ir; m.mehrgardi@gmail.com; Fax: +98 3116689732; Tel: +98 3117932710

† Electronic supplementary information (ESI) available. See DOI: 10.1039/c4an01171f

detection procedures (*e.g.*, multiple redox cycling) or conjugation chemistries (*e.g.*, labeling of enzymes and nanoparticles, *etc.*). Developing new technologies with improved simplicity, selectivity, and sensitivity for DNA hybridization detection that do not require complicated fabrication, instrumentation, and additional reagents is still a major challenge.

Graphene nanosheet (GN), single-layer carbon atoms densely packed into a two-dimensional honeycomb lattice, is the newest member of the carbon materials family.[26–29] Because of its excellent electrical, mechanical, chemical and sensing performance,[30–33] GN has been used in various electrochemical applications. GNs are hydrophobic and aggregate in aqueous media.[34,35] To improve their solubility in water, GNs are oxidized to graphene oxide (GO) by generating surface carboxylic acid and hydroxyl groups. Recent studies have demonstrated that GNs and GO can bind to single-stranded DNA (ss-DNA) *via* strong interactions, including van der Waals forces, π–π stacking, and/or hydrogen bonding.[36–41] These unique GN or GO/ss-DNA interactions have shown fascinating applications in gene diagnosis, protein analysis, and intracellular tracking.[42,43] However, the exploration of these unique interactions in electrochemical biosensing is still in the early stages. To the best of our knowledge, the electrochemical detection of SNPs based on a GO on NPGE platform has not been reported. In the present manuscript, GO is introduced as an insulating indicator of electrochemical signal for the detection of SNPs. As shown in Scheme 1, probe oligonucleotides were first immobilized on NPGE surface *via* Au–S chemistry. After hybridization with the target and the two times more concentrated complementary (2X Com) oligonucleotides to convert all single-stranded probe DNA to double stranded form, the un-hybridized parts of target or Com oligonucleotides can strongly interact with GO *via* strong π–π interaction. This causes a large increase in the charge transfer resistance (R_{ct}) because of the insulating property of GO and negatively charged backbone of DNA. However, the hybridization of capture oligonucleotides would inhibit GO interactions with the electrode. Therefore, R_{ct} was diminished but the decrease in the mutant targets is less than that for the Com targets because of less effective hybridization. Based on this strategy, a simple electrochemical DNA biosensor was fabricated for the sensitive detection of SNPs using GO on NPGE platform.

2. Materials and methods

2.1 Materials and reagents

All the oligonucleotides used for this study were obtained from Eurofins/MWG/Operon (Germany) with the following sequences (5′ to 3′): probe: SH–$(CH_2)_6$–CTG CGT TTT; capture: TTT TCG GCA; non-complementary: ACG AGC TAC; target oligonucleotides: complementary (Com): TGC CGA AAA AAA ACG CAG; A–C mismatch: TAC CGA AAA AAA ACG CAG and G–T mismatch: TGC TGA AAA AAA ACG CAG. Stock solutions of the oligonucleotides were prepared using a PBS buffer solution (pH 7.4) containing 0.01 M Na_2HPO_4, 0.002 M KH_2PO_4, 0.15 M NaCl and 0.15 M KCl, and were kept frozen at −20 °C. Analytical grade tris(2-carboxyethyl)phosphine (TCEP), 6-mercaptohexanol (MCH), sodium chloride, potassium chloride, magnesium chloride, sodium dihydrogen phosphate, disodium hydrogen phosphate, hydrochloric acid, nitric acid, sulfuric acid, potassium ferrocyanide and ferricyanide, and ascorbic acid were purchased from commercial sources (Merck or Sigma). Triply distilled water was used throughout the experiments.

2.2 Instrumental

All the electrochemical experiments were carried out using an Autolab PGSTAT30 (ECO Chemie, The Netherlands, driven by GPES4.9 software). The detection was performed in a home-made[44] electrochemical cell containing small parts of gold recordable compact disks (CDtrode) as the working electrode, an Ag/AgCl/3M KCl as the reference electrode and a platinum wire as the auxiliary electrode. Electrochemical impedance spectroscopy (EIS) and voltammetric measurements were performed in a solution containing $K_3[Fe(CN)_6]$–$K_4[Fe(CN)_6$ (1 : 1, 0.5 mM) and KCl (0.1 M). EIS measurements were performed by applying an AC potential with a signal amplitude of 5 mV and a frequency range of 10 kHz to 0.1 Hz at open circuit potential (OCP). Scanning electron microscopy (SEM) was accomplished on a PHILIPS XL-30 ESEM at an accelerating voltage of 20 kV. X-ray diffraction (XRD) patterns of the samples were recorded on a Bruker D8/Advance X-ray diffractometer with Cu-K_α radiation at 40 kV and 40 mA. Absorbance was measured using a JASCOV-670 UV-Vis. spectrophotometer. Thermogravimetric analysis (TGA) of graphite and graphene oxide was carried out under N_2 flow using thermogravimetric analyzer Q50 (USA) and their masses were recorded as a function of temperature. The samples were heated from room temperature to 600 °C at a rate of 10 °C min^{-1}. FT-IR spectra were recorded using JASCO, FT/IR-6300 (Japan) and surface Raman spectra were collected on a SENTERRA Raman spectrometer using 745 nm laser excitation.

2.3 Preparation of NPGE

A piece of a CD was cut off and the protective layer was removed by putting it in concentrated nitric acid according to a previously reported procedure.[18,45–47] Then, it was thoroughly washed with water. Subsequently, the CDtrode was electrochemically cleaned with 0.01 M NaOH and 0.05 M H_2SO_4 (**1**). NPGE (**2**) was prepared in two steps according to previous methods.[9,18] In the first step, the gold surface electrode was anodized by applying a step potential of 3.6 V in a phosphate buffer solution (pH 7.4) for 3 min. In the second step, the anodized gold surface was reduced to metallic Au for 5 min using 1.0 M of ascorbic acid as a non-toxic and low-cost reducing agent. The color of the CDtrode surface became darker due to the formation of a nanoporous structure.

2.4 Preparation of GO

Graphene oxide (GO) was synthesized from natural graphite powder by a modified Hummers method that has been previously reported by Shi *et al.*[48] Briefly, 3 g graphite powder was put into 12 mL concentrated H_2SO_4 (80 °C), 2.5 g $K_2S_2O_8$, and 2.5 g P_2O_5 for 4.5 h. Then, the mixture was filtered and washed with DI water to remove any residual acid. Pretreated graphite

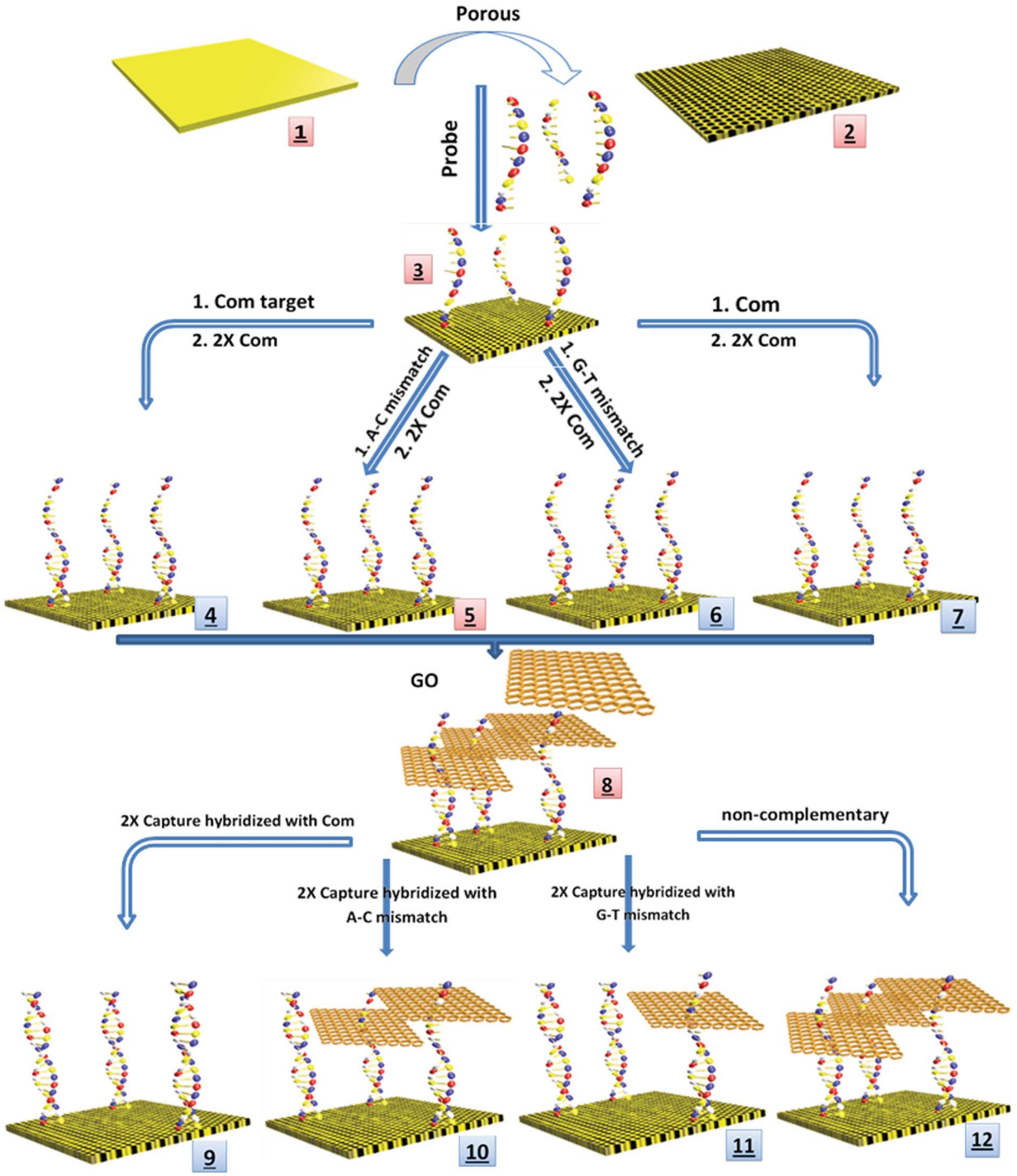

Scheme 1 Schematic presentation of different modification steps for the fabrication of a graphene oxide-based nanoporous gold electrode platform.

powder was put into 120 mL cold (0 °C) concentrated H_2SO_4. Then, 15 g $KMnO_4$ was added gradually under stirring at 20 °C temperature and the solution was diluted to 700 mL. Subsequently, 20 mL of 30% H_2O_2 was added to the mixture. In this step, the color of the mixture changed to brilliant yellow along with an intensive release of bubbles. The mixture was then filtered and washed with a 1 : 10 HCl aqueous solution (~1 L) to remove metal ions followed by a gentle wash to remove the acid. Exfoliation was carried out by sonicating a 0.1 mg mL^{-1} GO dispersion under ambient conditions for 30 min. The resulting homogeneous yellow-brown dispersion exhibits high stability over several months.

2.5 Modification of NPGE

The thiolated probe was freshly prepared and disulfide bonds were reduced using TCEP solution. In a typical procedure, first,

a 20 μL aliquot of 6 μM probe with 4 μL of 0.5 mM TCEP was incubated in dark for 1 h and was subsequently dropped on NPGE at room temperature for 16 h to self-assemble the probes on NPGE through Au–S chemistry. The probe-modified electrode was then washed using 10 mM PBS (pH 7.40) to remove non-specifically adsorbed probes on the surface. 10 μL of 5 μM MCH aqueous solution was put on the CDtrode surface to further eliminate the non-adsorbed DNA molecules. Subsequently, 12 μL of the different concentrations of target oligonucleotides along with 4 μL of 2 M magnesium chloride were dropped on the MCH/probe-modified electrode (**3**). After washing this MCH/probe/target NPGE (MCH/probe/Com (**4**), MCH/probe/A–C mismatch (**5**) and MCH/probe/G–T mismatch (**6**)), a drop containing 12 μL of the complementary target (12 μM, two-times more concentrated than the probe; 2X Com) oligonucleotide was added to the electrodes and allowed to react for 2 h to enable complete hybridization. After that, 12 μL of 0.1 mg mL^{-1} GO was dropped on the electrode surface and left for 1 h (GO-treated target modified (**8**)). In the next step, a drop containing 12 μL of 12 μM capture (again two-times more concentrated than the probe; 2X capture) oligonucleotide, and 2 μL of 2 M magnesium chloride were placed on the NPGE surface. Control experiment was carried out with a non-complementary oligonucleotide.

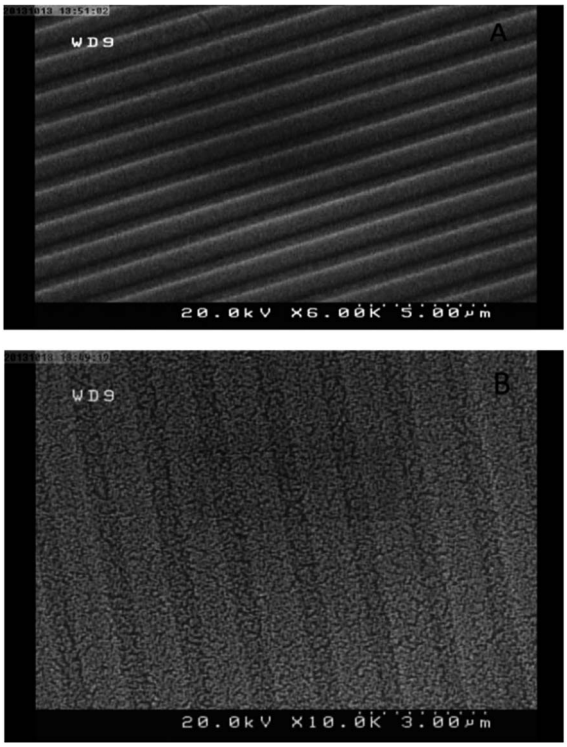

Fig. 1 SEM images of bare gold (A) and NPGE (B).

3. Results and discussion

3.1 Characterization of NPGE

High surface area NPGE has attracted significant interest for their applications as biosensors. Compared with untreated gold electrodes, the NPGEs possess considerably higher surface areas and better electron transfer, which offer a numerous adsorption sites for DNA, proteins and enzymes.[8,9] The surface areas of the untreated gold electrode (**1**) and NPGE (**2**) were measured by following their cyclic voltammograms in 0.5 M sulfuric acid. By assuming a specific charge of 386 μC cm^{-1} for the reduction of one monolayer of gold oxide to metallic gold,[49] the electroactive surface areas of the (**1**) and (**2**) electrodes obtained are equal to 0.21 ± 0.03 cm^2 and 1.2 ± 0.20 cm^2, respectively. These values represent ~6 times increase in the active area of the electrode after converting it to nanoporous. Fig. 1 shows the SEM images of both the (**1**) and (**2**) electrodes. The image of the surface of (**2**) reveals a nanoporous structure, while that of the (**1**) substrate shows a smooth structure with parallel data storage grooves.

3.2 Characterization of GO

The SEM image of GO (Fig. S1A†) illustrates that the exfoliation of GO was accomplished with the formation of very thin layers with flake-like structures. As shown in Fig. S1B,† the feature diffraction peak of exfoliated GO appears at 11.4° (002) with an inter-distance (*d*-spacing) of 7.75 A°. This value is larger than the *d*-spacing (3.35 A°) of pristine graphite ($2\theta = 26.6°$) because of the presence of oxygen containing functional groups.[50] The UV-Vis spectrum (Fig. S1C†) of yellow-brown GO shows a distinct absorption peak at 230 nm due to the π–π* transition of C=C bonds, which is attributed to the characteristic absorption of GO.[50,51] Fig. S2† shows the FT-IR spectra of graphene oxide. The presence of different types of oxygen functionalities in graphene oxide were confirmed at 3400 cm^{-1} (O–H stretching vibrations), 1720 cm^{-1} (stretching vibrations from C=O), 1600 cm^{-1} (skeletal vibrations from unoxidized graphitic domains), 1220 cm^{-1} (C–OH stretching vibrations), and 1060 cm^{-1} (C–O stretching vibrations).[52] The results of TGA are shown in Fig. S3.† As expected, graphite was highly stable up to 600 °C. Graphene oxide shows a slight mass decrease from room temperature to 150 °C and a significant decrease from 150 °C to 200 °C. The mass of graphene oxide further decreased slowly up to 600 °C. Major mass reduction at ~200 °C was caused by the pyrolysis of oxygen-containing functional groups, generating CO, CO_2 and steam.[53] As shown in Fig. S4,† the Raman spectrum of GO displays two prominent peaks at 1600 and 1360 cm^{-1}, which correspond to the well-documented G and D bands.[54]

3.3 Effect of pH on the interaction of GO with ss-DNA

To facilitate the interaction of GO with the aromatic hydrophobic rings of DNA bases through π–π stacking, electrostatic repulsion between the DNA and the negatively charged GO surface must be overcome. Therefore, controlling the surface charge of GO by changing the pH of the solution is a key parameter in the response of biosensor. For this purpose, several PBS solutions with different pH over a range of 4–8 were prepared. The adsorption of GO on immobilized DNA strands on electrode surface at different pH were followed by the

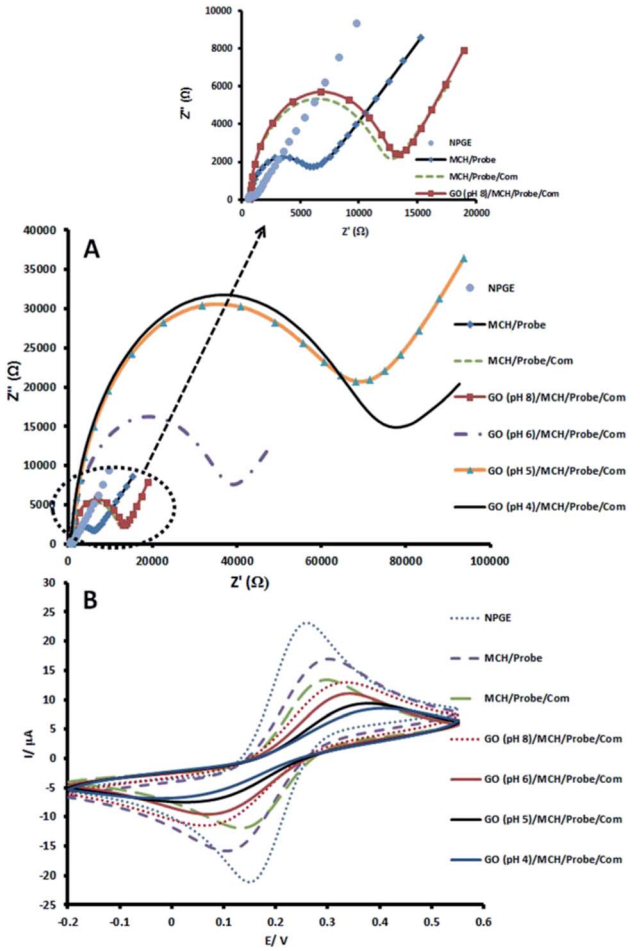

Fig. 2 Nyquist plots (A) and CVs (B) obtained for NPGE (**2**), MCH/probe (**3**), MCH/probe/Com (**4**) and GO-treated Com/NPGE (**5**) after exposure to different pH GO solutions.

incubation of the MCH/probe/Com electrode (**4**) for 1 h at different pH and recording the EIS spectra and voltammograms of the redox $[Fe(CN)_6]^{3-/4-}$ couple on NPGE. Because GO is an insulator, charge transfer to the redox couple was expected to be more difficult after accumulation of GO on the surface. Fig. 2A and B show that the R_{ct} of EIS and the peak separation of voltammograms for the redox couple increased significantly after the exposure of (**4**) to a GO solution at lower pH. Based on these results, pH 4 was selected to be the optimum pH for detection. The GO surface is terminated by several different oxygen-containing groups on its surface, and the pK_a values of these groups should be close to that of benzoic acid (p$K_a = 4.2$) or acetic acid (p$K_a = 4.7$).[40,55] At neutral pH, these groups are deprotonated to give a highly negatively charged surface but closer to the pK_a; the surface charge is neutralized. The surface charge is neutralized to reduce repulsion; under these conditions, π–π interactions or hydrophobic interactions dominate.

3.4 Quantization of surface coverage of DNA immobilization

The surface coverage of the probe-modified NPGE was determined by a protocol previously reported by Steel *et al.*[56] Briefly, the chronocoulometric signals of the modified NPGE were followed in the presence and absence of a cationic redox reporter, ruthenium hexamine trichloride (RuHex), that is electrostatically bound to the negatively charged DNA backbone. After the immobilization of probes on the electrode surface, the probe-modified electrode was subjected to RuHex. Then, the amount of RuHex was measured by chronocoulometry using the Cottrell equation. DNA surface density was obtained using the following equation:

$$\Gamma_{DNA} = \Gamma_0 \left(\frac{z}{m}\right) N_A$$

Where Γ_{DNA} is the probe surface density in molecules per cm^2, m is the number of bases in probe DNA, z is the charge of RuHex and N_A is the Avogadro's number. The obtained surface density of the probe DNA is equal to 5.2 ($\pm$0.5) $\times$ 10^{12} molecules per cm^2.

3.5 Electrochemical detection of SNPs on NPGE

This assay has been designed for discriminating between various SNPs based on the less effective hybridization of mismatch targets compared to complementary targets and the differences between the interactions of GO sheets with ss-DNA and ds-DNA. If the entire DNA probe strands on the electrode surface are not hybridized with their complementary bases, GO can interact with their free bases. To avoid this problem, after the addition of different concentrations of targets, 2X Com was

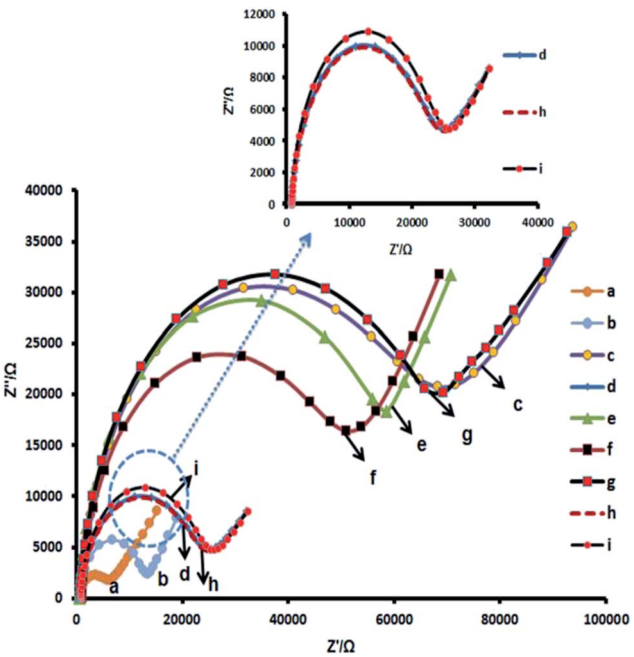

Fig. 3 Nyquist plots recorded on the electrode surface (**3**) (a), MCH/probe/target (**4**, **5**, **6**) (b), GO-treated targets (**8**) (c), capture hybridized with Com target (**9**) (d), with A–C mismatch (**10**) (e), with G–T mismatch (**11**) (f) and negative control with a non-complementary sequence (**12**) (g). MCH/probe/Com (**4**) after treatment of capture without GO and (h). MCH/probe/Com (**4**) first reacted with capture oligonucleotide and then incubated with 0.1 mg mL^{-1} GO for 1 h (i).

dropped on the electrode surface. It is worth mentioning that the lower sections of the complementary and mismatch targets are entirely the same and complementary with the probe sequence. Fig. 3 (spectrum a) shows the EIS using $Fe(CN)_6^{3-}$/$Fe(CN)_6^{4-}$ as the redox probe on the surface of MCH/probe/NPGE (**3**). Upon hybridization of the probe with mismatch or complementary targets followed by treatment with excess complementary target (2X com), the negative charges on the surface are developed (**4** or **5** or **6**) and R_{ct} is increased (spectrum b). Because the hybridizing segment of different targets with the probe is the same, no significant differences in EIS were observed on the surface of **4**, **5** or **6**.

By treating the MCH/probe/target NPGE surface with GO sheets, strong interactions with the non-hybridized moieties of the targets *via* π–π interactions (**8**) cause dramatic increases in R_{ct} because of the hindrance introduced by the adsorption of insulating GO on electrode surface (spectrum c). In the next step, by the hybridization of capture oligonucleotides with a non-hybridized section of the Com (**9**), A–C (**10**) or G–T mismatch (**11**), charge transfer resistances were decreased (spectra of d, e and f respectively), while the treatment of the surface with non-complementary target does not significantly change R_{ct} (spectrum (g)).

The treatment of a complementary target with 2X capture (**9**) shows the greatest decrease in the resistance (spectrum d). This R_{ct} is the most similar to resistance observed for the same surface without treatment with GO sheets (spectrum h). This demonstrates that for the Com targets hybridization is approximately complete and all of the GO sheets leave the surface. In addition, the hybridization of the Com target with 2X capture followed by treatment with GO sheets does not significantly change R_{ct} (spectrum i). This is further evidence to demonstrate that there is no interaction between ds-DNA and GO and there is no nonspecific adsorption of GO on the ss-DNA probe. On the other hand, R_{ct} for the A–C and G–T mismatch targets (**10 and 11**) is also decreased by treating the surface with 2X capture but this decrease is not as large as the decrease in the R_{ct} of the Com target (spectra e and f) that can be attributed to the less effective hybridization of mismatch targets. Another important point observed here is the difference between the R_{ct} of the A–C (**10**) and G–T mismatches (**11**) (spectra e and f). The G–T mismatch is thermodynamically more stable than the A–C mismatch. Therefore, the hybridization of the G–T mismatches is more effective than that of the A–C mismatches and is less effective than that of the complementary targets such that there would be more GO remaining on the surface than in the case of Com targets and less than in the case of the A–C mismatch targets. This causes a larger R_{ct} compared to the Com targets (spectrum d) and a smaller R_{ct} compared to the A–C mismatch targets (spectrum f). Finally, for non-complementary targets (**12**) no significant changes in R_{ct} (spectrum g) are observed compared to the surface (**8**).

As shown in Fig. 4, when the concentration of G–T mismatches is increased, R_{ct} is also increased. This can be attributed to the less effective hybridization of G–T mismatches compared to the Com targets, which causes more interaction between the insulating GO and the non-hybridized section of

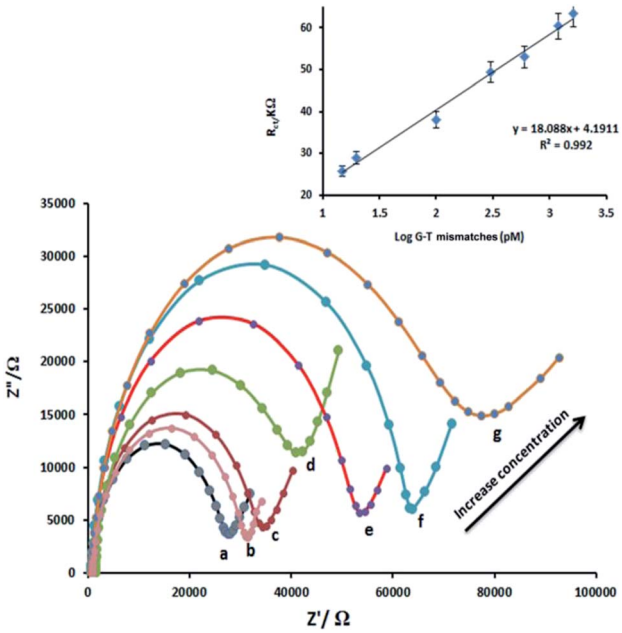

Fig. 4 Nyquist plots for EIS detection of various concentrations (a: 15; b: 20; c: 100; d: 300; e: 600; f: 1200; and g: 1600 (pM)) of thermodynamically stable G–T mismatches on GO-treated G–T mismatches (**11**). (Inset) the resulting calibration curve.

the G–T mismatches, gradually increasing the R_{ct}. There is a logarithmic relationship between R_{ct} and G–T mismatch concentrations over the range of 15–1600 pM (inset Fig. 4). Therefore, the presented method could be successfully applied for the detection and quantification of different SNPs at low concentration levels.

Finally, to demonstrate that reduction in resistance only originates from the hybridization process and not, for example, from the instability of GO sheets on the surface; their stabilities were investigated by recording 50 cyclic voltammograms on the

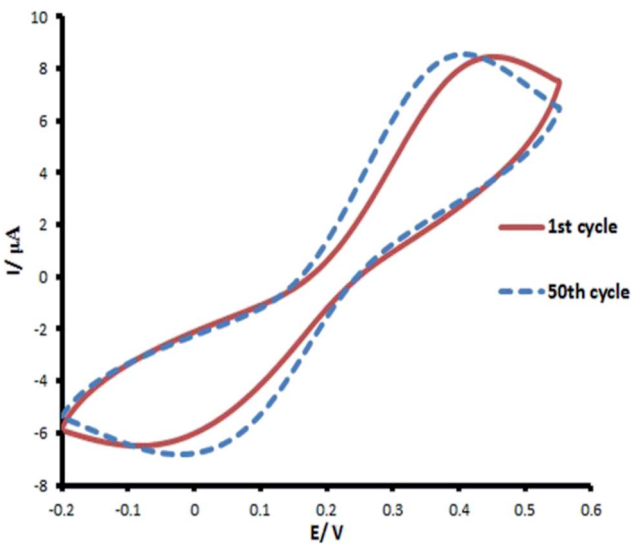

Fig. 5 Stability of GO-treated Com NPGE (**8**) after 50 cycles.

GO-treated Com (**8**). Fig. 5 demonstrates that GO sheets on the surface (**4**) are very stable, which shows the almost unchanged redox peak currents of $[Fe(CN)_6]^{3-/4-}$.

4. Conclusion

Efficient, simple and highly sensitive electrochemical DNA biosensors have been developed by taking advantage of NPGE, soluble graphene oxide (GO), and unique GO/ss-DNA interaction for the detection of DNA hybridization and polymorphism using EIS. On the basis of the differences between the interactions of ss-DNA and dsDNA with GO, different SNPs have been successfully detected, including a thermodynamically stable G–T mismatch with a dynamic range of 15–1600 pM. The GO-based electrochemical biosensing NPGE platform has clear advantages over the conventional method. First, NPGE provided a high loading immobilized platform. Second, by combining the soluble insulation of GO and unique GO/ss-DNA interaction, a label-free detection strategy is realized, which makes the sensing process very simple and convenient. Finally, because GO can be prepared from low cost graphite, the GO-based method is cost-effective.

Acknowledgements

We gratefully acknowledge the support of this work by the University of Isfahan Research Council.

References

1 R. Salari, C. Kimchi-Sarfaty, M. M. Gottesman and T. M. Przytycka, *Nucleic Acids Res.*, 2013, **41**, 44–53.
2 G. Liu, T. M. Lee and J. Wang, *J. Am. Chem. Soc.*, 2005, **127**, 38–39.
3 K. B. Cederquist, R. Stoermer Golightly and C. D. Keating, *Langmuir*, 2008, **24**, 9162–9171.
4 T. H. Kjallman, H. Peng, C. Soeller and J. Travas-Sejdic, *Anal. Chem.*, 2008, **80**, 9460–9466.
5 F. P. Zamborini, L. Bao and R. Dasari, *Anal. Chem.*, 2011, **84**, 541–576.
6 H. Cai, C. Xu, P. He and Y. Fang, *J. Electroanal. Chem.*, 2001, **510**, 78–85.
7 L. Soleymani, Z. Fang, E. H. Sargent and S. O. Kelley, *Nat. Nanotechnol.*, 2009, **4**, 844–848.
8 K. Hu, D. Lan, X. Li and S. Zhang, *Anal. Chem.*, 2008, **80**, 9124–9130.
9 L. E. Ahangar and M. A. Mehrgardi, *Biosens. Bioelectron.*, 2012, **38**, 252–257.
10 H. Qiu, L. Xue, G. Ji, G. Zhou, X. Huang, Y. Qu and P. Gao, *Biosens. Bioelectron.*, 2009, **24**, 3014–3018.
11 H. Qiu, C. Xu, X. Huang, Y. Ding, Y. Qu and P. Gao, *J. Phys. Chem. C*, 2009, **113**, 2521–2525.
12 H. Qiu, Y. Li, G. Ji, G. Zhou, X. Huang, Y. Qu and P. Gao, *Bioresour. Technol.*, 2009, **100**, 3837–3842.
13 A. Huczko, *Appl. Phys. A*, 2000, **70**, 365–376.
14 Q. Yi and W. Yu, *J. Electroanal. Chem.*, 2009, **633**, 159–164.
15 J. F. Huang and I. W. Sun, *Adv. Funct. Mater.*, 2005, **15**, 989–994.
16 F. Li, X. Han and S. Liu, *Biosens. Bioelectron.*, 2011, **26**, 2619–2625.
17 W. Huang, M. Wang, J. Zheng and Z. Li, *J. Phys. Chem. C*, 2009, **113**, 1800–1805.
18 A. Kiani and E. N. Fard, *Electrochim. Acta*, 2009, **54**, 7254–7259.
19 H. Qiu and X. Huang, *J. Electroanal. Chem.*, 2010, **643**, 39–45.
20 L. Kashefi-Kheyrabadi and M. A. Mehrgardi, *Bioelectrochemistry*, 2013, **94**, 47–52.
21 M. J. Shiddiky, M. A. Rahman, C. S. Cheol and Y.-B. Shim, *Anal. Biochem.*, 2008, **379**, 170–175.
22 F. Patolsky, A. Lichtenstein and I. Willner, *Angew. Chem., Int. Ed.*, 2000, **39**, 940–943.
23 S. Liu, P. Wu, W. Li, H. Zhang and C. Cai, *Anal. Chem.*, 2011, **83**, 4752–4758.
24 T. Selvaraju, J. Das, K. Jo, K. Kwon, C.-H. Huh, T. K. Kim and H. Yang, *Langmuir*, 2008, **24**, 9883–9888.
25 J. A. Hansen, R. Mukhopadhyay, J. Ø. Hansen and K. V. Gothelf, *J. Am.Chem. Soc.*, 2006, **128**, 3860–3861.
26 F. Kim, L. J. Cote and J. Huang, *Adv. Mater.*, 2010, **22**, 1954–1958.
27 C. N. R. Rao, A. K. Sood, K. S. Subrahmanyam and A. Govindaraj, *Angew. Chem., Int. Ed.*, 2009, **48**, 7752–7777.
28 A. K. Geim and K. S. Novoselov, *Nat. Mater.*, 2007, **6**, 183–191.
29 S. Guo, D. Wen, Y. Zhai, S. Dong and E. Wang, *ACS Nano*, 2010, **4**, 3959–3968.
30 M. J. Allen, V. C. Tung and R. B. Kaner, *Chem. Rev.*, 2009, **110**, 132–145.
31 D. R. Dreyer, S. Park, C. W. Bielawski and R. S. Ruoff, *Chem. Soc. Rev.*, 2010, **39**, 228–240.
32 D. Chen, L. Tang and J. Li, *Chem. Soc. Rev.*, 2010, **39**, 3157–3180.
33 Y. Wang, Y. Shao, D. W. Matson, J. Li and Y. Lin, *ACS Nano*, 2010, **4**, 1790–1798.
34 H. Bai, Y. Xu, L. Zhao, C. Li and G. Shi, *Chem. Commun.*, 2009, 1667–1669.
35 J. Long, M. Fang and G. Chen, *J. Mater. Chem.*, 2011, **21**, 10421–10425.
36 N. Varghese, U. Mogera, A. Govindaraj, A. Das, P. K. Maiti, A. K. Sood and C. Rao, *ChemPhysChem*, 2009, **10**, 206–210.
37 C. H. Lu, H. H. Yang, C. L. Zhu, X. Chen and G. N. Chen, *Angew. Chem.*, 2009, **121**, 4879–4881.
38 Y. Wang, Z. Li, D. Hu, C.-T. Lin, J. Li and Y. Lin, *J. Am. Chem. Soc.*, 2010, **132**, 9274–9276.
39 L. Wang, M. Xu, L. Han, M. Zhou, C. Zhu and S. Dong, *Anal. Chem.*, 2012, **84**, 7301–7307.
40 H. Park, S.-J. Hwang and K. Kim, *Electrochem. Commun.*, 2012, **24**, 100–103.
41 L. Tang, Y. Wang, Y. Liu and J. Li, *ACS Nano*, 2011, **5**, 3817–3822.
42 B. Gulbakan, E. Yasun, M. I. Shukoor, Z. Zhu, M. You, X. Tan, H. Sanchez, D. H. Powell, H. Dai and W. Tan, *J. Am. Chem. Soc.*, 2010, **132**, 17408–17410.
43 A. Bonanni and M. Pumera, *ACS Nano*, 2011, **5**, 2356–2361.

44 L. E. Ahangar and M. A. Mehrgardi, *Electrochim. Acta*, 2011, **56**, 10264–10269.
45 L. Angnes, E. M. Richter, M. A. Augelli and G. H. Kume, *Anal. Chem.*, 2000, **72**, 5503–5506.
46 M. A. Mehrgardi and L. E. Ahangar, *Biosens. Bioelectron.*, 2011, **26**, 4308–4313.
47 S. M. Khoshfetrat and M. A. Mehrgardi, *ChemElectroChem*, 2014, **1**, 779–786.
48 Y. Xu, H. Bai, G. Lu, C. Li and G. Shi, *J. Am. Chem. Soc.*, 2008, **130**, 5856–5857.
49 R. Szamocki, A. Velichko, C. Holzapfel, F. Mücklich, S. Ravaine, P. Garrigue, N. Sojic, R. Hempelmann and A. Kuhn, *Anal. Chem.*, 2007, **79**, 533–539.
50 H.-L. Guo, X.-F. Wang, Q.-Y. Qian, F.-B. Wang and X.-H. Xia, *ACS Nano*, 2009, **3**, 2653–2659.
51 D. Li, M. B. Müller, S. Gilje, R. B. Kaner and G. G. Wallace, *Nat. Nanotechnol.*, 2008, **3**, 101–105.
52 E.-Y. Choi, T. H. Han, J. Hong, J. E. Kim, S. H. Lee, H. W. Kim and S. O. Kim, *J. Mater. Chem.*, 2010, **20**, 1907–1912.
53 S. Stankovich, D. A. Dikin, R. D. Piner, K. A. Kohlhaas, A. Kleinhammes, Y. Jia, Y. Wu, S. T. Nguyen and R. S. Ruoff, *Carbon*, 2007, **45**, 1558–1565.
54 D. Graf, F. Molitor, K. Ensslin, C. Stampfer, A. Jungen, C. Hierold and L. Wirtz, *Nano Lett.*, 2007, **7**, 238–242.
55 Y. Miyake, H. Togashi, M. Tashiro, H. Yamaguchi, S. Oda, M. Kudo, Y. Tanaka, Y. Kondo, R. Sawa and T. Fujimoto, *J. Am. Chem. Soc.*, 2006, **128**, 2172–2173.
56 A. B. Steel, T. M. Herne and M. J. Tarlov, *Anal. Chem.*, 1998, **70**, 4670–4677.

